Received: Added at production | Revised: Added at production | Accepted: Added at production

DOI: xxx/xxxx

SHORT REPORT

Sensitivity of unconstrained quantitative magnetization transfer MRI to Amyloid burden in preclinical Alzheimer's disease

Andrew Mao[1,1,1] | **Sebastian Flassbeck**[1,1] | **Elisa Marchetto**[1,1] | **Arjun V. Masurkar**[1,1,1] | **Henry Rusinek**[1,1,1,1] | **Jakob Assländer**[1,1]

[1]Bernard and Irene Schwartz Center for Biomedical Imaging, Department of Radiology, New York University Grossman School of Medicine, New York, New York, USA

[2]Center for Advanced Imaging Innovation and Research (CAI^{2}R), Department of Radiology, New York University Grossman School of Medicine, New York, New York, USA

[3]Vilcek Institute of Graduate Biomedical Sciences, New York University Grossman School of Medicine, New York, New York, USA

[4]Alzheimer's Disease Research Center, Center for Cognitive Neurology, New York University Grossman School of Medicine, New York, New York, USA

[5]Department of Neurology, New York University Grossman School of Medicine, New York, New York, USA

[6]Department of Neuroscience and Physiology, New York University Grossman School of Medicine, New York, New York, USA

[7]Department of Psychiatry, New York University Grossman School of Medicine, New York, New York, USA

Correspondence
Corresponding author: Andrew Mao,
Email: andrew.mao@nyumc.org

Abstract

Introduction: Magnetization transfer MRI is sensitive to semi-solid macromolecules, including amyloid beta, and has been used to discriminate Alzheimer's disease (AD) patients from controls. Here, we utilize an unconstrained 2-pool quantitative MT (qMT) approach that quantifies the longitudinal relaxation rates $R_1^{f,s}$ of free water and semi-solids separately, and investigate its sensitivity to amyloid accumulation in preclinical subjects.

Methods: We recruited 15 cognitively normal subjects, of which nine were amyloid positive by [^{18}F]Florbetaben PET. A 12 min qMT scan was used to estimate the unconstrained 2-pool qMT parameters. Group comparisons and correlations were analyzed at the lobar level.

Results: The exchange rate and semi-solid pool's R_1^s were sensitive to the amyloid concentration. The former finding is consistent with previous reports in clinical AD, but the latter is novel as its value is typically constrained.

Discussion: qMT MRI may be a promising surrogate marker of amyloid beta without the need for contrast agents or radiotracers.

KEYWORDS

Alzheimer's disease, amyloid-beta, magnetic resonance imaging, magnetization transfer, florbetaben, positron emission tomography

1 | INTRODUCTION

Amyloid β (Aβ) is one of the defining pathological hallmarks of Alzheimer's disease (AD)[1] which begins accumulating in the neocortex[2] even in clinically asymptomatic subjects.[3] Identifying individuals with a substantial amyloid load is necessary for many clinical reasons, including the specific diagnosis of AD versus other dementias,[1] and to study the impact of new disease-modifying therapies—such as emerging anti-amyloid immunotherapeutics—which are being used to treat early stages of AD and increasingly being studied in preclinical patient populations.[4]

Abbreviations: qMT, quantitative magnetization transfer. **Word Count**: 2481.

The gold standard for *in vivo* amyloid assessment is Positron Emission Tomography (PET). PET offers high sensitivity for *in situ* amyloid,[5] and radiotracer injection is less invasive than lumbar puncture-based measurement of cerebrospinal fluid (CSF) amyloid biomarkers. However, PET has several drawbacks, including cost, the need for specialized equipment, limited spatial resolution, off-target binding and ionizing radiation exposure. In this work, we investigate an alternative, magnetic resonance imaging (MRI)-based technique called quantitative magnetization transfer (qMT),[6] depicted in Fig. 1. MT methods sensitize the MRI signal to a "semi-solid" pool consisting of large macromolecules such as lipids (e.g., myelin) and proteins (e.g., both $A\beta_{40}$ and $A\beta_{42}$ aggregates), which exchanges with the usual free water pool. MT's sensitivity to Aβ plaque

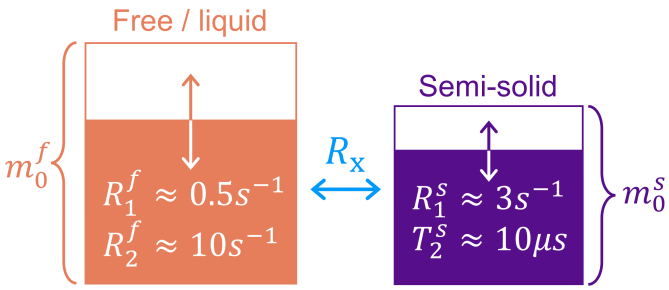

FIGURE 1 2-pool quantitative magnetization transfer model.[6,13] The red-colored pool models "free water" protons with fraction m_0^f, while macromolecule-bound "semi-solid" protons with fraction m_0^s are colored purple ($m_0^s + m_0^f = 1$). Each pool's longitudinal and transverse relaxation rates (reciprocal of the times) $R_1^{f,s}$ and $R_2^{f,s}$, respectively, are modeled separately (most previous studies constrain the value of R_1^s). After saturation of one pool's longitudinal magnetization, relaxation and exchange with the other pool modulate each pool's magnetization as visualized by the arrows and partially colored boxes. The exchange rate is denoted by R_x.

accumulation was previously demonstrated in transgenic mice,[7,8,9] and *in vivo* studies using *quantitative* MT—which disentangles the biophysical contributions to the MT contrast—suggest that the "forward magnetization exchange rate" (the product $m_0^s \cdot R_x$, Fig. 1) is the most discriminatory qMT biomarker for classifying AD versus controls and the conversion to AD from amnestic mild cognitive impairment (MCI).[10,11,12]

However, due to previous works' focus on MCI or clinical AD,[10,11,12] it is unclear whether preclinical AD pathology can be detected with qMT biomarkers. In this study, we focus on the preclinical population where amyloid accumulation is believed to occur before tau hyperphosphorylation and neurodegeneration.[3] Additionally, prior qMT studies usually constrain the value of the difficult-to-estimate semi-solid pool's longitudinal relaxation rate R_1^s.[10,11] In this work, we quantify all parameters of the unconstrained 2-pool qMT model using advances in biophysical modeling.[13] Our central hypothesis is that amyloid accumulation in the preclinical population is detectable by qMT biomarkers—including R_1^s—due to the distinct biochemical properties of Aβ plaques.

2 | METHODS

2.1 | Magnetization Transfer Model

The unconstrained 2-pool qMT model (Fig. 1) models the MRI signal as arising from protons bound in free water (superscript ^{f}) which exchange magnetization at the rate R_x with protons bound in a semi-solid pool (superscript ^{s}). Each pool has its own fractional size ($m_0^{f,s}$, where $m_0^s + m_0^f = 1$), longitudinal ($R_1^{f,s}$) and transverse ($R_2^{f,s}$) relaxation rates (inverse of times $T_{1,2}$), amounting to six total parameters: $m_0^s, R_1^f, R_2^f, R_x, R_1^s$, and T_2^s. Previous studies[10,11,12] could not estimate m_0^s and R_x separately due to limitations of the employed encoding strategies and signal models,[14] which we overcome here by utilizing a hybrid-state sequence[15] (see Section 2.3).

We use the time T_2^s (instead of the rate) for consistency with the qMT literature, which is characterized by the super-Lorentzian lineshape[16] and modeled with the generalized Bloch equations.[17] As $T_2^s \approx 10\,\mu$s, the semi-solid pool can be detected only indirectly with clinical MRI scanners via its exchange with the free pool, impeding estimation of R_1^s. This leads authors to typically assume $R_1^s = 1$ s in the literature.[10,11] However, we recently demonstrated the ability to quantify R_1^s voxel-wise,[13] which takes on significantly smaller values than R_1^f.[18,19] We hypothesized that eliminating this constraint increases qMT's sensitivity to changes in the semi-solid pool's biophysical properties arising from Aβ accumulation.

2.2 | Participants

We recruited 15 cognitively normal subjects (Clinical Dementia Rating® of 0) who previously received amyloid PET scans from New York University's AD Research Center (ADRC) cohort of community-dwelling elderly adults. Six were considered Aβ− by our ADRC's standardized uptake value ratio (SUVR) threshold, with the demographics: three female, three white, age 72.6 ± 4.5 years (mean ± standard deviation), Montreal Cognitive Assessment (MoCa) scores 27.3 ± 2.2, one *APOE*-ε4 and two *APOE*-ε2 carriers. The remaining nine subjects were Aβ+, with the demographics: five female, seven white, age 75.6 ± 6.5 years, MoCa 27.4 ± 2.4, six *APOE*-ε4 carriers. All subjects provided written informed consent for the studies below.

2.3 | Imaging Protocol

All subjects received 300 MBq of [^{18}F]florbetaben (FBB) tracer (Life Molecular Imaging, Totowa, NJ) intravenously, followed by a saline flush. Syringes were assayed pre- and post-injection. Amyloid PET scans were acquired on a Biograph mMR PET/MRI system (Siemens, Germany) 90–120 minutes post-injection.

In a second session 17±9 months (no more than 34 months) later, each subject underwent a 24 minute MRI exam on a Prisma MRI scanner (Siemens, Germany) using a 32-channel head coil. Our experimental whole-brain qMT technique used a hybrid-state sequence[15] optimized for quantifying MT parameters with 1 mm isotropic resolution (effectively 1.24 mm isotropic accounting for 3D radial k-space sampling) across a 256×256×256 mm FOV in 12 minutes.[13] Hybrid-state sequences build on inversion-recovery balanced steady-state free precession (bSSFP) sequences[20] by incorporating a smoothly varying flip angle between TRs to improve biophysical parameter encoding.[15] Full details and example parameter maps can be found in Ref.[13].

3D Magnetization-Prepared Rapid Acquisition Gradient-Recalled Echo (MPRAGE)[21] and T2-weighted Fluid-Attenuated Inversion-Recovery (FLAIR)[22] images were also acquired with 1 mm isotropic resolution. Both sequences were GRAPPA 2x accelerated, where the MPRAGE used a

TE/TR/TI of 2.98 ms/2.3 s/900 ms for 5 min 30 s of scan time and the FLAIR used a TE/TR/TI of 392 ms/5 s/1.8 s for 5 min 57 s of scan time.

2.4 | Image Reconstruction

PET reconstruction used slightly modified SCAN parameters (https://scan.naccdata.org/): single-frame of first 10 mins of data (to reduce motion-related artifacts); OSEM-3D, 4 iterations, 21 subsets; 344×344×127 grid; 2.0 zoom (1.04313×1.04313×2.03125 mm voxels); all corrections on; post-reconstruction smoothing with a 2 mm FWHM gaussian kernel.[23] Attenuation correction used an MR-based algorithm combining a Dixon μ-map with a superimposed, co-registered, skull atlas-derived bone compartment.[23]

qMT parameter maps were estimated using a two-step procedure.[24] First, a series of "coefficient images," representing the MRI signal's temporal dynamics, was reconstructed[25] using an information-maximizing subspace[26] with motion corrected in 4 s intervals.[27] Then, the six qMT parameters are estimated using a neural network designed with similar properties to least-squares estimators incorporating a data-driven correction for magnetic field inhomogeneities.[28]

2.5 | Image Processing

The MPRAGE, FLAIR, and FBB images were rigid-body registered[29] to the estimated m_0^s maps (which has a similar contrast to the MPRAGE). The qMT parameters were chosen as the common reference frame to avoid interpolating the non-linearly processed qMT maps. Brain segmentation, cortical parcellation, volume, and thickness values were then computed using Freesurfer v7.4.1's "recon-all" command.[30,31] Volumes were normalized by the estimated total intracranial volume, and the average global cerebellar FBB value was used to compute SUVRs.

As the cortical thickness is only 2–3 voxels for our image resolutions, to minimize partial volume effects, we used Freesurfer's "mri_vol2surf" function to sample the qMT and FBB SUVR values at 50% of the cortical thickness. To avoid resampling the non-linearly processed qMT data and minimize linear interpolation error, we applied the following procedure. First, we sinc interpolated[32] the reconstructed coefficient images onto a 5× finer grid (i.e., 0.2×0.2×0.2 mm voxels). Then, we applied "mri_vol2surf" to sample the coefficient images at 50% of the cortical depth before applying the neural network to estimate the qMT parameters.

Due to small sample sizes, we perform a lobar-level analysis by grouping the Desikan-Killiany ROIs[33] into the four primary cortical lobes.[34] Each subject's average measurement (qMT parameter, FBB SUVR, or cortical thickness) per lobe and hemisphere is computed using an inverse-variance weighting[35] based on each ROI's sample variance. Prior to all statistical analyses, we manually excluded four ROIs (for all measurements) where we identified substantial artifacts in R_x across multiple subjects: the rostral anterior cingulate, precentral, postcentral, and superior parietal gyri. We also excluded three ROIs (for all measurements) superior to the frontal sinus exhibiting bSSFP-like banding artifacts[20] in the qMT parameters: the medial and lateral orbitofrontal cortex and temporal pole.

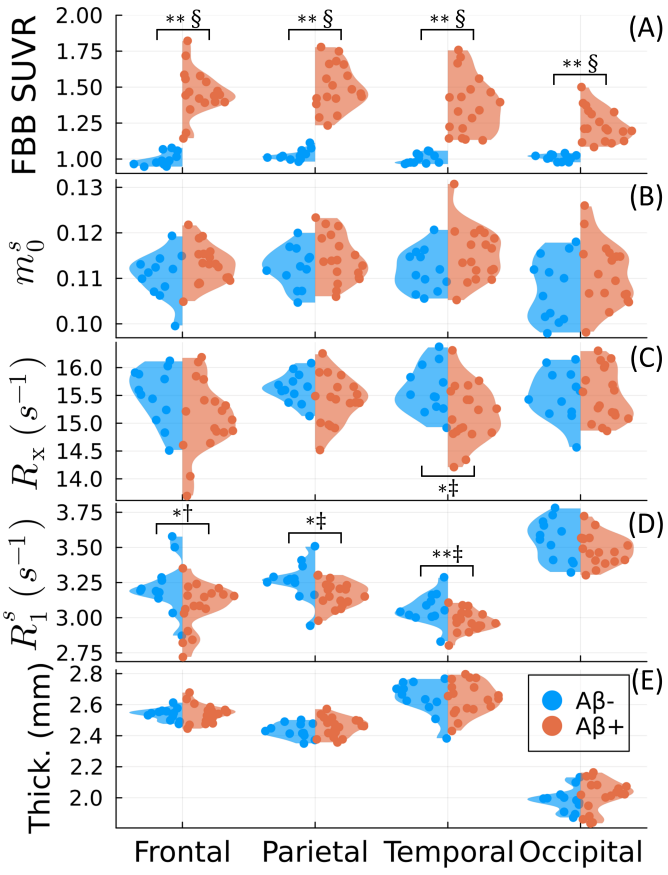

FIGURE 2 Group comparison. [^{18}F]florbetaben (FBB) SUVR (A), three qMT parameters (the macromolecular pool size m_0^s (B), the magnetization exchange rate R_x (C), and the macromolecular pool's longitudinal relaxation rate R_1^s (D)), and cortical thickness (E) are compared between amyloid negative (Aβ−) and positive (Aβ+) groups. $*$ and $**$ denote statistical significance for $p < 0.05$ and the Bonferroni-corrected $p < 0.0125$, respectively, using the Mann-Whitney U test.[36] †, ‡, and § indicate medium, large and very large effect sizes using Hedge's g,[37,38] respectively.

2.6 | Statistical Analysis

We used the non-parametric Mann-Whitney U test[36] to compare measurements between Aβ− and Aβ+ groups. We considered the $p < 0.05$ and Bonferroni-corrected $p < 0.0125$ (across the four lobes) significance levels. Effect sizes were quantified using Hedge's g,[37] where we considered $0 \leq |g| < 0.5$ "small," $0.5 \leq |g| < 0.8$ "medium," $0.8 \leq |g| < 1.2$ "large," and $|g| \geq 1.2$ "very large."[38] We used Pearson's correlation coefficient to evaluate the association of our measurements with amyloid burden, again using the $p < 0.05$ significance level.

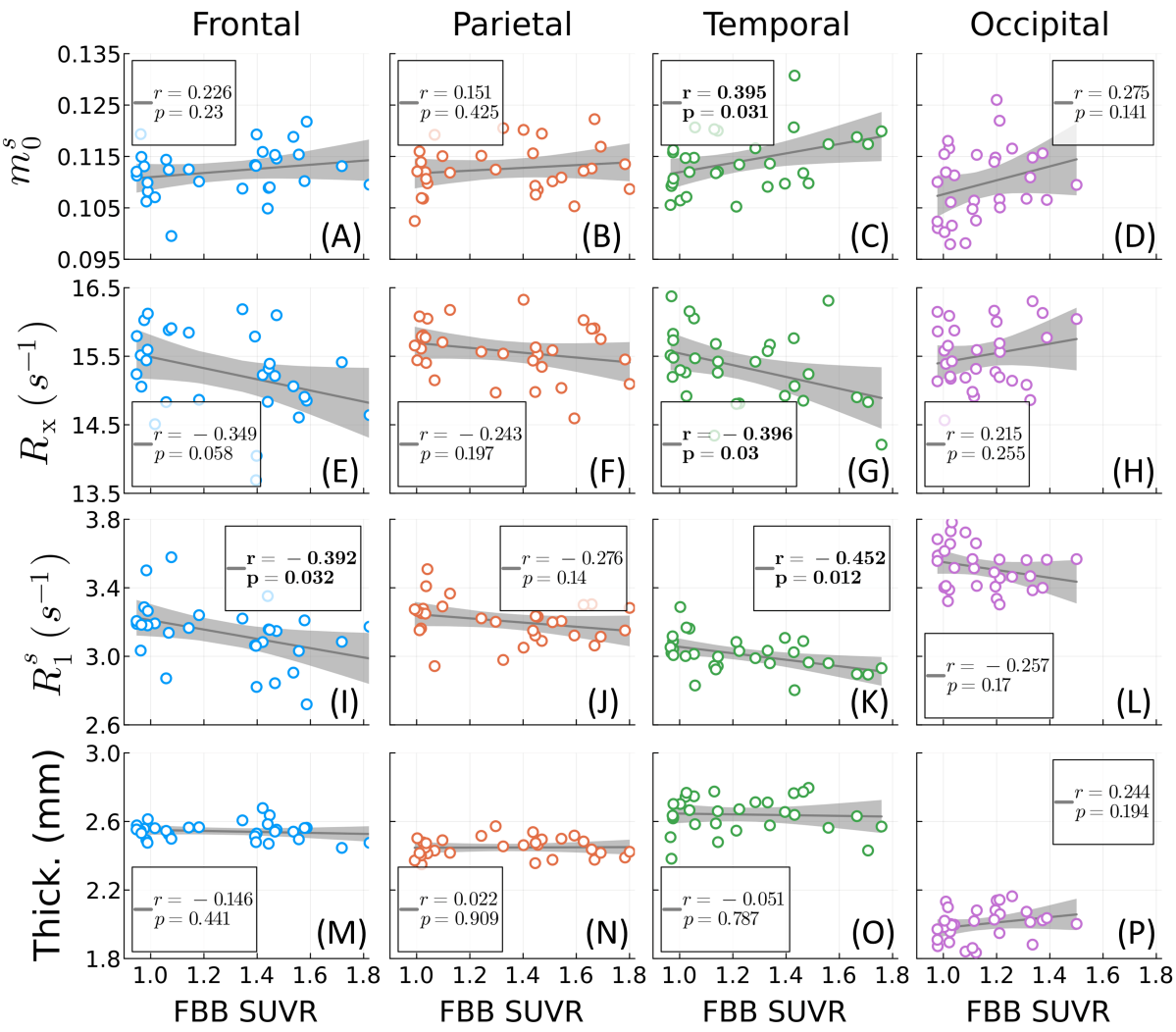

FIGURE 3 Correlation analysis. Three qMT parameters—the macromolecular pool size m_0^s (A–D), the magnetization exchange rate R_x (E–H), and the macromolecular pool's longitudinal relaxation rate R_1^s (I–L)—and cortical thickness (M–P) are plotted against amyloid burden as measured by [^{18}F]florbetaben (FBB) PET SUVR. Significant Pearson's correlations ($p < 0.05$) are bolded.

3 | RESULTS

Fig. 2 compares the qMT parameters, FBB SUVR, and cortical thickness values between Aβ− and Aβ+ groups. SUVR values were uniformly significantly increased for Aβ+ subjects with very large effect sizes, as expected from our definition of amyloid positivity. Consistent with previous literature reports, the magnetization exchange rate R_x was significantly decreased in the temporal lobe with a large effect size ($g = -0.86$). The macromolecular pool's longitudinal relaxation rate R_1^s was significantly decreased in the frontal, parietal, and temporal lobes with medium ($g = -0.78$), large ($g = -0.81$) and large ($g = -0.94$) effect sizes, respectively. By contrast, no significant group differences were observed in any lobe for the macromolecular pool size m_0^s, cortical thickness (including treating the "cortical signature"[39] as a lobe), total CSF volumes, or remaining qMT parameters (the latter are not shown).

We repeated the same analysis for the Freesurfer-defined global white matter and subcortical structures (not shown). While there were no differences in the subcortical structure volumes (including the hippocampus[40]), we observed significant decreases in both free pool relaxation times (R_1^f and R_2^f) in the global white matter, hippocampus, and thalamus.

Fig. 3 analyzes the correlation between the qMT parameters or cortical thickness and amyloid concentration. Significant Pearson's correlations occur in similar locations to Fig. 2, though there was no significant negative correlation with R_1^s in the parietal lobe, but a significant positive correlation with m_0^s in the temporal lobe. Similarly to Fig. 2, no significant correlations were observed between cortical thickness and amyloid concentration in any lobe (neither for the composite "cortical signature"[39]).

To understand the spatial correspondence between the qMT measurements and FBB SUVR, we visualize the corresponding effect sizes overlaid on the Desikan-Killiany atlas in Fig. 4. As expected, very large

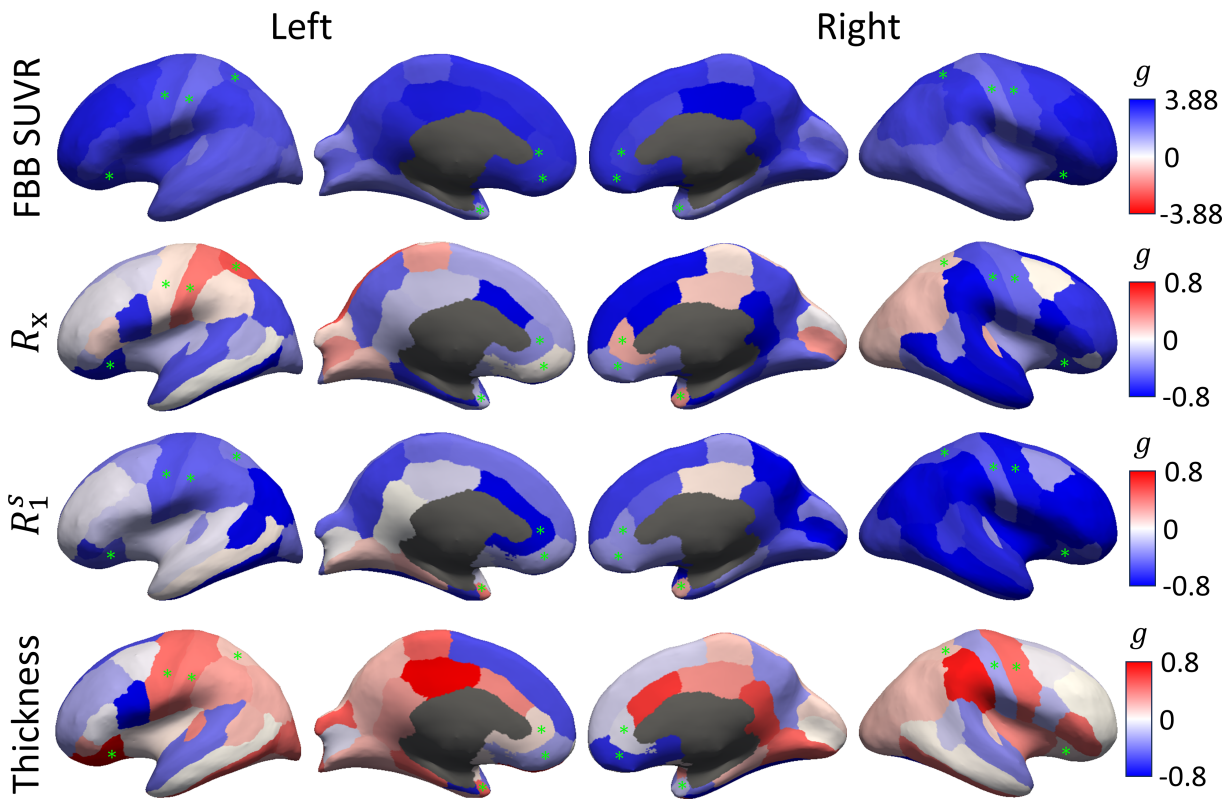

FIGURE 4 Effect sizes. Hedge's g[37] comparing Aβ− and Aβ+ groups is overlaid on the Desikan-Killiany surface atlas[33] for the magnetization exchange rate R_x, the macromolecular pool's longitudinal relaxation rate R_1^s, and cortical thickness in comparison to [^{18}F]florbetaben (FBB) PET SUVR. A positive effect size ($g > 0$) means measurements are larger in the Aβ+ group, and $|g| = 0.8$ (a "large" effect[38]) is used as an illustrative cutoff. For FBB SUVR, note the modified cutoffs using the maximal $|g|$ value (due to very large positive effect sizes) and the reversed colorbar, used to color the expected direction of effects as blue for all measures (positive for FBB SUVR, negative for R_x, R_1^s, and thickness). The green asterisks denote ROIs excluded from the lobar-level analyses for all measures in Figs. 2–3.

positive effect sizes are uniformly observed across the cortex for FBB SUVR. While we do not observe uniformly large *negative* effect sizes for R_x and R_1^s, the ROIs exhibiting (likely spurious) *positive* effects somewhat overlap with the ROIs excluded from the lobar analyses for exhibiting imaging artifacts (e.g., the postcentral and superior parietal gyri in R_x). Importantly, though we do observe small ($g = -0.42$) to medium ($g = -0.69$) effects suggesting thinning of the right/left entorhinal cortices,[39,40] the qMT parameters exhibit higher overall sensitivity to amyloid burden.

4 | DISCUSSION

Our study revealed widespread group differences in unconstrained qMT parameters between Aβ+ and Aβ− individuals. The largest effect was observed in the semi-solid pool's longitudinal relaxation rate R_1^s, a parameter previously considered inaccessible and hence typically constrained—but which we quantify on a voxel-by-voxel basis using the hybrid-state's enhanced signal encoding capabilities.[13,15,41] This suggests that R_1^s may be a potential biomarker for amyloid pathology preceding morphometric measures of atrophy.[39,40] A potential biophysical explanation could be the slower longitudinal relaxation of spins bound in Aβ plaques relative to other constituents of the macromolecular pool, e.g., myelin.

We also observed an R_x reduction in Aβ+ subjects, which has previously been attributed to the hydrophobicity of Aβ plaques.[10] This finding aligns with previous reports that the forward exchange rate (i.e., $m_0^s \cdot R_x$) is reduced in *clinical* AD and predictive of amnestic MCI to AD conversion.[10,11,12] Our results using an *unconstrained* qMT model, however, suggest that R_x is more sensitive to amyloid pathology than m_0^s in *preclinical* AD. If neurodegeneration causes reduced m_0^s in advanced disease (discussed further in Section 4.2), R_x and m_0^s may potentially be associated with the 'A' and 'N' axes of the A/T/N framework,[1] respectively, which emphasizes the importance of separating these parameters in the unconstrained model.

Contrary to our expectations of an increase with greater amyloid burden, we found no significant group differences in the macromolecular pool size m_0^s, although a positive correlation was observed in the temporal lobe. One explanation could be a competing effect, possibly due to concomitant neurodegeneration or a change in the interstitial load of water (e.g., due to reduced fluid clearance[42] or vascular leakage from reactive astrogliosis[43]). However, the latter hypothesis appears less likely

given the lack of significant changes we would expect in the free water pool's relaxation rates R_1^f and R_2^f.[13,44]

4.1 | Limitations

Our study has several limitations. Firstly, a larger cohort is needed to verify our findings, control for the effect of nuisance variables (e.g., age, sex, race), and increase statistical power for ROI or voxel-level analyses (partially overcome here by sampling at 50% of the cortical depth). Secondly, mechanistic studies are needed to elucidate the specific pathophysiological processes underpinning the observed changes in R_x and R_1^s, including potential covariates like blood-brain barrier breakdown,[42] temperature,[45] or pH changes.[46] For example, altered perfusion could explain the decreased R_2^f observed in subcortical structures and white matter. Temperature differences of even 1–2 °C could explain the observed cortical differences in R_x and R_1^s.[47] pH changes due to mitochondrial dysfunction[48] would decrease R_x and may have preceded cognitive decline in our cohort. Additionally, a post-mortem study of the relationship between R_x/R_1^s and plaque density (diffuse, neuritic and vascular) would provide a stronger histopathological basis for our data. Lastly, our findings should be validated in preclinical (e.g., mouse) models of AD, as our unconstrained model differs from the existing literature primarily utilizing constrained qMT approaches.[7,8,9]

4.2 | Future Directions

Our proof-of-concept study was based on a prototype qMT sequence originally designed for the study of white matter. Future work will involve optimizing the sequence for grey matter imaging. Further, the qMT maps had artifacts particularly affecting ROIs in the frontal and parietal lobes, which could explain their relative lack of significant effects compared to the temporal lobe. Future work will involve correcting for the chemical shift of subcutaneous fat, a likely source of artifacts given the employed radial k-space trajectory.

The qMT sequence has an effective 1.24 mm isotropic resolution. Future work will explore the potential advantages of this high resolution (as compared to PET) in the study of finer structures relevant to AD, e.g., the hippocampus and cortex.

Unconstrained qMT should also be extended to study injury in white matter[11] where m_0^s was previously demonstrated to be closely associated with myelin content,[49,50] but amyloid PET has significant off-target binding.[5] Additionally, we hypothesize that grey matter neurodegeneration in clinical AD would also be reflected by reduced m_0^s. This motivates further investigation into which unconstrained qMT parameters might be sensitive to disease progression. Under the model of amyloid accumulation and progressive neurodegeneration as temporally displaced processes,[3] qMT's potential sensitivity to both 'A' and 'N' axes[1] could improve the specificity for and monitoring of AD stage.

qMT—which combines high-resolution anatomical imaging and amyloid sensitivity in a single exam—may also be useful for the longitudinal monitoring of therapeutic response in clinical trials. In particular, emerging immunotherapeutics are increasingly being studied in preclinical patient populations; e.g., in AHEAD 3-45.[4] Importantly, both forms of amyloid-related imaging abnormalities (ARIA) are likely detectable in the free water relaxation rates (and not R_x or R_1^s).[13,44] While the qMT effect sizes are substantially smaller than those of amyloid PET, qMT is more amenable to screening, longitudinal imaging, and multi-center studies by virtue of being implementable on existing MRI scanners.

5 | CONCLUSION

qMT is a minimal addition to routinely used conventional MRI, and may enable the detection of amyloid accumulation without requiring contrast agents or radiotracers.

ACKNOWLEDGMENTS

The authors like to thank David H. Salat, Ryn Flaherty and Yu Veronica Sui for their helpful pointers regarding the use of the Freesurfer package, and Zena Rockowitz for her assistance with subject recruitment.

SOURCES OF FUNDING

This work was supported by NIH grants F30 AG077794, R01 NS131948, T32 GM136573, an NIA-funded Alzheimer's Disease Research Center (P30 AG066512), and was performed under the rubric of the Center for Advanced Imaging Innovation and Research (CAI2R), an NIBIB National Center for Biomedical Imaging and Bioengineering (P41 EB017183).

DISCLOSURES

None reported.

CONSENT STATEMENT

Informed consent was obtained from all study participants in agreement with the requirements of our institution's IRB.

REFERENCES

1. Jack CR, Bennett DA, Blennow K, Carrillo MC, Dunn B, Haeberlein SB, et al. NIA-AA Research Framework: Toward a biological definition of Alzheimer's disease. *Alzheimer's and Dementia*. 2018;14(4):535–562. doi: 10.1016/j.jalz.2018.02.018
2. Fantoni E, Collij L, Alves IL, Buckley C, Farrar G. The spatial-temporal ordering of amyloid pathology and opportunities for PET imaging. *Journal of Nuclear Medicine*. 2020;61(2):166–171. doi: 10.2967/jnumed.119.235879
3. Jack CR, Knopman DS, Jagust WJ, Shaw LM, Aisen PS, Weiner MW, et al. Hypothetical model of dynamic biomarkers of the Alzheimer's pathological cascade. *The Lancet Neurology*. 2010;9(1):119–128. doi: 10.1016/S1474-4422(09)70299-6
4. Yadollahikhales G, Rojas JC. Anti-Amyloid Immunotherapies for Alzheimer's Disease: A 2023 Clinical Update. *Neurotherapeutics*. 2023;20(4):914–931. doi: 10.1007/s13311-023-01405-0
5. Chapleau M, Iaccarino L, Soleimani-Meigooni D, Rabinovici GD. The Role of Amyloid PET in Imaging Neurodegenerative Disorders: A Review. *Journal of Nuclear Medicine*. 2022;63:13S–19S. doi: 10.2967/jnumed.121.263195
6. Henkelman RM, Huang X, Xiang Q, Stanisz GJ, Swanson SD, Bronskill MJ. Quantitative interpretation of magnetization transfer. *Magnetic Resonance in Medicine*. 1993;29(6):759–766. doi: 10.1002/mrm.1910290607
7. Pérez-Torres CJ, Reynolds JO, Pautler RG. Use of Magnetization Transfer Contrast MRI to Detect Early Molecular Pathology in Alzheimer's Disease. *Magnetic Resonance in Medicine*. 2014;71(1):333–338. doi: 10.1002/mrm.24665
8. Bigot C, Vanhoutte G, Verhoye M, Van der Linden A. Magnetization transfer contrast imaging reveals amyloid pathology in Alzheimer's disease transgenic mice. *NeuroImage*. 2014;87:111–119. doi: 10.1016/j.neuroimage.2013.10.056
9. Praet J, Bigot C, Orije J, Naeyaert M, Shah D, Mai Z, et al. Magnetization transfer contrast imaging detects early white matter changes in the APP/PS1 amyloidosis mouse model. *NeuroImage: Clinical*. 2016;12:85–92. doi: 10.1016/j.nicl.2016.06.014
10. Giulietti G, Bozzali M, Figura V, Spanò B, Perri R, Marra C, et al. Quantitative magnetization transfer provides information complementary to grey matter atrophy in Alzheimer's disease brains. *NeuroImage*. 2012;59(2):1114–1122. doi: 10.1016/j.neuroimage.2011.09.043
11. Makovac E, Serra L, Di Domenico C, Marra C, Caltagirone C, Cercignani M, et al. Quantitative Magnetization Transfer of White Matter Tracts Correlates with Diffusion Tensor Imaging Indices in Predicting the Conversion from Mild Cognitive Impairment to Alzheimer's Disease. *Journal of Alzheimer's Disease*. 2018;63(2):561–575. doi: 10.3233/JAD-170995
12. Duan W, Sehrawat P, Zhou TD, Becker JT, Lopez OL, Gach HM, et al. Pattern of Altered Magnetization Transfer Rate in Alzheimer's Disease. *Journal of Alzheimer's Disease*. 2022;88(2):693–705. doi: 10.3233/JAD-220335
13. Assländer J, Mao A, Marchetto E, Beck ES, La Rosa F, Charlson RW, et al. Unconstrained quantitative magnetization transfer imaging: disentangling T1 of the free and semi-solid spin pools. *arXiv*. 2023. doi: 10.48550/arXiv.2301.08394
14. Ramani A, Dalton C, Miller DH, Tofts PS, Barker GJ. Precise estimate of fundamental in-vivo MT parameters in human brain in clinically feasible times. *Magnetic Resonance Imaging*. 2002;20(10):721–731. doi: 10.1016/S0730-725X(02)00598-2
15. Assländer J, Novikov DS, Lattanzi R, Sodickson DK, Cloos MA. Hybrid-state free precession in nuclear magnetic resonance. *Communications Physics*. 2019;2(1):73. doi: 10.1038/s42005-019-0174-0
16. Morrison C, Stanisz G, Henkelman R. Modeling Magnetization Transfer for Biological-like Systems Using a Semi-solid Pool with a Super-Lorentzian Lineshape and Dipolar Reservoir. *Journal of Magnetic Resonance, Series B*. 1995;108(2):103–113. doi: 10.1006/jmrb.1995.1111
17. Assländer J, Gultekin C, Flassbeck S, Glaser SJ, Sodickson DK. Generalized Bloch model: A theory for pulsed magnetization transfer. *Magnetic Resonance in Medicine*. 2021(July):1–15. doi: 10.1002/mrm.29071
18. Helms G, Hagberg GE. In vivo quantification of the bound pool T1 in human white matter using the binary spin-bath model of progressive magnetization transfer saturation. *Physics in Medicine and Biology*. 2009;54(23). doi: 10.1088/0031-9155/54/23/N01
19. Manning AP, MacKay AL, Michal CA. Understanding aqueous and non-aqueous proton T1 relaxation in brain. *Journal of Magnetic Resonance*. 2021;323:106909. doi: 10.1016/j.jmr.2020.106909
20. Bieri O, Scheffler K. Fundamentals of balanced steady state free precession MRI. *Journal of Magnetic Resonance Imaging*. 2013;38(1):2–11. doi: 10.1002/jmri.24163
21. Brant-Zawadzki M, Gillan GD, Nitz WR. MP RAGE: a three-dimensional, T1-weighted, gradient-echo sequence–initial experience in the brain. *Radiology*. 1992;182(3):769–775. doi: 10.1148/radiology.182.3.1535892
22. Hajnal JV, Coene BD, Lewis PD, Baudouin CJ, Cowan FM, Pennock JM, et al. High Signal Regions in Normal White Matter Shown by Heavily T2-Weighted CSF Nulled IR Sequences. *Journal of Computer Assisted Tomography*. 1992;16(4):506–513. doi: 10.1097/00004728-199207000-00002
23. Koesters T, Friedman KP, Fenchel M, Zhan Y, Hermosillo G, Babb J, et al. Dixon sequence with superimposed model-based bone compartment provides highly accurate PET/MR attenuation correction of the brain. *Journal of Nuclear Medicine*. 2016;57(6):918–924. doi: 10.2967/jnumed.115.166967
24. Assländer J. A Perspective on MR Fingerprinting. *Journal of Magnetic Resonance Imaging*. 2021;53(3):676–685. doi: 10.1002/jmri.27134
25. Assländer J, Cloos MA, Knoll F, Sodickson DK, Hennig J, Lattanzi R. Low rank alternating direction method of multipliers reconstruction for MR fingerprinting. *Magnetic Resonance in Medicine*. 2018;79(1):83–96. doi: 10.1002/mrm.26639
26. Mao A, Flassbeck S, Gultekin C, Assländer J. Cramér-Rao Bound Optimized Subspace Reconstruction in Quantitative MRI. *arXiv*. 2023. doi: 10.48550/arXiv.2305.00326
27. Flassbeck S, Marchetto E, Mao A, Assländer J. Contrast-Optimized Basis Functions for Self-Navigated Motion Correction in 3D quantitative MRI. *Proc. Intl. Soc. Mag. Reson. Med.*. 2024.
28. Mao A, Flassbeck S, Assländer J. Bias-Reduced Neural Networks for Parameter Estimation in Quantitative MRI. *arXiv*. 2023. doi: 10.48550/arXiv.2312.11468
29. Reuter M, Rosas HD, Fischl B. Highly accurate inverse consistent registration: A robust approach. *NeuroImage*. 2010;53(4):1181–1196. doi: 10.1016/j.neuroimage.2010.07.020
30. Fischl B, Salat DH, Busa E, Albert M, Dieterich M, Haselgrove C, et al. Whole Brain Segmentation. *Neuron*. 2002;33(3):341–355. doi: 10.1016/s0896-6273(02)00569-x
31. Fischl B. Automatically Parcellating the Human Cerebral Cortex. *Cerebral Cortex*. 2004;14(1):11–22. doi: 10.1093/cercor/bhg087
32. Oppenheim AV, Willsky AS. *Signals and Systems*. Upper Saddle River, NJ: Pearson. 2 ed., 1996.
33. Desikan RS, Ségonne F, Fischl B, Quinn BT, Dickerson BC, Blacker D, et al. An automated labeling system for subdividing the human cerebral cortex on MRI scans into gyral based regions of interest. *NeuroImage*. 2006;31(3):968–980. doi: 10.1016/j.neuroimage.2006.01.021
34. Klein A, Tourville J. 101 Labeled Brain Images and a Consistent Human Cortical Labeling Protocol. *Frontiers in Neuroscience*. 2012;6(DEC):1–12. doi: 10.3389/fnins.2012.00171
35. Kay SM. *Fundamentals of Statistical Signal Processing, Volume I: Estimation Theory*. Philadelphia, PA: Prentice Hall, 1993.

36. Fay MP, Proschan MA. Wilcoxon-Mann-Whitney or T-test? on assumptions for hypothesis tests and multiple interpretations of decision rules. *Statistics Surveys*. 2010;4:1–39. doi: 10.1214/09-SS051
37. Hedges LV. Distribution Theory for Glass's Estimator of Effect size and Related Estimators. *Journal of Educational Statistics*. 1981;6(2):107–128. doi: 10.3102/10769986006002107
38. Sawilowsky SS. New Effect Size Rules of Thumb. *Journal of Modern Applied Statistical Methods*. 2009;8(2):597–599. doi: 10.22237/jmasm/1257035100
39. Dickerson BC, Stoub TR, Shah RC, Sperling RA, Killiany RJ, Albert MS, et al. Alzheimer-signature MRI biomarker predicts AD dementia in cognitively normal adults. *Neurology*. 2011;76(16):1395–1402. doi: 10.1212/WNL.0b013e3182166e96
40. Sabuncu MR, Desikan RS, Sepulcre J, Yeo BTT, Liu H, Schmansky NJ, et al. The dynamics of cortical and hippocampal atrophy in Alzheimer disease. *Archives of Neurology*. 2011;68(8):1040–1048. doi: 10.1001/archneurol.2011.167
41. Assländer J, Gultekin C, Mao A, Zhang X, Duchemin Q, Liu K, et al. Rapid quantitative magnetization transfer imaging: Utilizing the hybrid state and the generalized Bloch model. *Magnetic Resonance in Medicine*. 2024;91(4):1478–1497. doi: 10.1002/mrm.29951
42. Tarasoff-Conway JM, Carare RO, Osorio RS, Glodzik L, Butler T, Fieremans E, et al. Clearance systems in the brain—implications for Alzheimer disease. *Nature Reviews Neurology*. 2015;11(8):457–470. doi: 10.1038/nrneurol.2015.119
43. Nakahara M, Hayashi H, Kumazaki T, Mori O. Value of magnetization transfer contrast as a sensitive technique to reflect histopathological changes in the white matter adjacent to the frontal horns of lateral ventricles. *Journal of Nippon Medical School*. 1999;66(4):245–252. doi: 10.1272/jnms.66.245
44. Stanisz GJ, Webb S, Munro CA, Pun T, Midha R. MR Properties of Excised Neural Tissue Following Experimentally Induced Inflammation. *Magnetic Resonance in Medicine*. 2004;51(3):473–479. doi: 10.1002/mrm.20008
45. Klegeris A, Schulzer M, Harper DG, McGeer PL. Increase in Core Body Temperature of Alzheimer's Disease Patients as a Possible Indicator of Chronic Neuroinflammation: A Meta-Analysis. *Gerontology*. 2006;53(1):7–11. doi: 10.1159/000095386
46. Louie EA, Gochberg DF, Does MD, Damon BM. Transverse relaxation and magnetization transfer in skeletal muscle: Effect of pH. *Magnetic Resonance in Medicine*. 2008;61(3):560–569. doi: 10.1002/mrm.21847
47. Birkl C, Langkammer C, Haybaeck J, Ernst C, Stollberger R, Fazekas F, et al. Temperature-induced changes of magnetic resonance relaxation times in the human brain: A postmortem study. *Magnetic Resonance in Medicine*. 2013;71(4):1575–1580. doi: 10.1002/mrm.24799
48. Wang W, Zhao F, Ma X, Perry G, Zhu X. Mitochondria dysfunction in the pathogenesis of Alzheimer's disease: Recent advances. *Molecular Neurodegeneration*. 2020;15(1):1–22. doi: 10.1186/s13024-020-00376-6
49. Janve VA, Zu Z, Yao SY, Li K, Zhang FL, Wilson KJ, et al. The radial diffusivity and magnetization transfer pool size ratio are sensitive markers for demyelination in a rat model of type III multiple sclerosis (MS) lesions. *NeuroImage*. 2013;74:298–305. doi: 10.1016/j.neuroimage.2013.02.034
50. Thiessen JD, Zhang Y, Zhang H, Wang L, Buist R, Del Bigio MR, et al. Quantitative MRI and ultrastructural examination of the cuprizone mouse model of demyelination. *NMR in Biomedicine*. 2013;26(11):1562–1581. doi: 10.1002/nbm.2992